ACS APPLIED MATERIALS & INTERFACES

Research Article

www.acsami.org

Oxygen-Rich Hierarchical Porous Carbon Derived from Artemia Cyst Shells with Superior Electrochemical Performance

Yufeng Zhao,*[,†,§] Wei Ran,[†] Jing He,[†] Yanfang Song,[‡] Chunming Zhang,[‡] Ding-Bang Xiong,[†] Faming Gao,[†] Jinsong Wu,*[,§] and Yongyao Xia[‡]

[†]Key Laboratory of Applied Chemistry, Yanshan University, Qinhuangdao 066004, China

[‡]Department of Chemistry, Fudan University, Shanghai 200433 China

[§]EPIC, NUANCE Center, Northwestern University 2220 Campus Drive, Evanston, Illinois 60208, United States

Supporting Information

ABSTRACT: In this study, three-dimensional (3D) hierarchical porous carbon with abundant functional groups is produced through a very simple low-cost carbonization of Artemia cyst shells. The unique hierarchical porous structure of this material, combining large numbers of micropores and macropores, as well as reasonable amount of mesopores, is proven favorable to capacitive behavior. The abundant oxygen functional groups from the natural carbon precursor contribute stable pseudocapacitance. As-prepared sample exhibits high specific capacitance (369 F g^{-1} in 1 M H_2SO_4 and 349 F g^{-1} in 6 M KOH), excellent cycling stability with capacitance retention of 100% over 10 000 cycles, and promising rate performance. This work not only describes a simple way to produce high-performance carbon electrode materials for practical application, but also inspires an idea for future structure design of porous carbon.

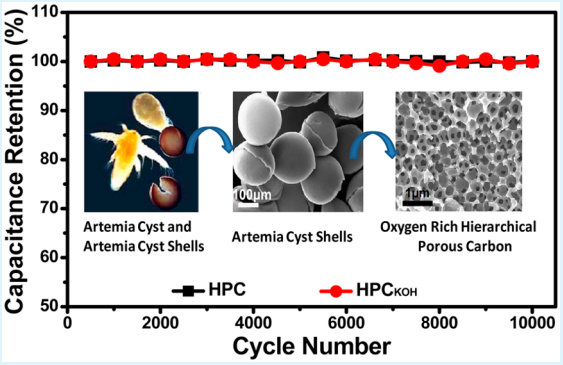

KEYWORDS: *oxygen-rich, carbon, hierarchical porous, natural carbon source, supercapacitor*

1. INTRODUCTION

Carbonaceous materials have attracted tremendous interest in the field of energy storage due to their relatively low cost, easy processability, and excellent physicochemical stability in different solutions (from strongly acidic to alkali).[1] Significant attention has been focused on the development of various carbon electrode materials, including activated carbon, carbon nanotubes (CNTs), carbon aerogels, carbide derived carbons (CDC), carbon nanofiber, graphene, and so on.[2−13] Among these materials, activated carbon with high microporosity has been most widely sought, due to its high specific surface area (SSA) and thus relatively high specific capacitance values. However, large numbers of micropores of the activated carbon have been typically considered to be inaccessible to electrolyte solutions, mainly because of their random pore connectivity and closure characteristics.[14−17] A number of approaches are devolving to optimize the specific capacitance (SC) of carbon materials and solve this problem. One effective approach is to develop carbon materials with three-dimensional (3D) hierarchical porous nanostructure, which can not only provide a continuous electron pathway, but can also facilitate ion transportation by shortening diffusion pathways.[18−21] Another approach is to introduce heteroatoms or graft oxygen-rich functional groups with pseudocapacitance.[22−25] The heteroatoms (N, O, B, S, P, etc.) or functional groups (carboxyl, ether, phenol, quinine, ketone, etc.) on the porous carbon wall can improve the wettability, contribute pseudocapacitance, and sometimes also enlarge the potential window.[22,23,26−28] Ideally, the 3D hierarchical porous carbon (HPC) with functionalized heteroatoms is desirable for high-performance supercapacitors. For example, Qie et al.[29] synthesized 3D hierarchical porous carbon with high-level heteroatom-doping, resulting in a high specific capacitance of 318.2 F g^{-1} was achieved. However, the conventional approach for functionalization is normally coupled with increasing cost and results in a tedious process and instability of pseudocapacitance properties given by functional groups when cycling the capacitors, especially in alkaline electrolytes.[30] A strong alternative approach is to directly use functional group enriched materials as the carbon precursor.[24] Biological carbon precursors from natural resources are generally renewable, inexpensive, and environmentally benign and are believed to be able to meet such demands.[31−39] Carbon derived from natural resources often possesses complicated and optimized hierarchical morphology with naturally perfect interconnection. For example, Lv et al.[37] prepared HPCs with SC of 184 F g^{-1} at a high current density of 10 A g^{-1} by using banana peels as a carbon source. Huang et al.[36] produced HPCs

Received: October 3, 2014
Accepted: December 22, 2014
Published: December 22, 2014

DOI: 10.1021/am506815f
ACS Appl. Mater. Interfaces 2015, 7, 1132−1139

with SC of 130 F g^{-1} at 100 A g^{-1} using animal bones as raw materials.

Artemia is a widely distributed small crustacean that lives in salt lakes, coastal salt flat pools, and other high salt fields, and large amount of Artemia cysts are marketed worldwide annually.[40,41] The cyst shell of this small crustacean possesses a hierarchical porous inner cortical structure.[40] Here, we report our use of a very simple carbonization process to produce 3D hierarchical porous carbon with abundant functional groups, using the waste Artemia cyst shells as a novel carbon source. Compared with other reported natural resource derived carbon, the as-prepared HPC exhibits an SC as high as 297 (6 M KOH) and 321 F g^{-1} (1 M H_2SO_4), good rate performance (above 90%), and particularly ultrastable performance upon cycling (100% retention after 10 000 cycles). The KOH activated HPC presents an even higher SC of 349 and 369 F g^{-1} in 6 M KOH and 1 M H_2SO_4, respectively.

2. EXPERIMENTAL SECTION

2.1. Preparation of HPC. Artemia cyst shells were cleaned with distilled water, dried at 80 °C for 24 h, and then ball-milled for 6 h at 300 rpm. The ball-milled Artemia cyst shells were then heated to 300 °C at Ar atmosphere with a heating rate of 1 °C min^{-1} and held at that temperature for 3 h. Then, they were heated to 700 °C at 1 °C min^{-1} and held at that temperature for 4 h. After that, the product was sonicated in 67 wt % HNO_3 for 80 min. After being cleaned and dried, the final product was obtained and denoted as HPC. By comparison, the carbon sample without HNO_3 treatment is denoted as $HPC_{untreated}$.

2.2. KOH Activation of HPC. The as-prepared HPC was mixed with KOH at weight ratio of 1:2 (W_{HPC}/W_{KOH}), and then heated to 700 °C at a heating rate of 10 °C min^{-1} in Ar atmosphere, held there for 1 h. The product was then washed in diluted HCl and distilled water and finally dried at 110 °C for 12 h. This product is denoted as HPC_{KOH}.

2.2. Materials Characterization. X-ray photoelectron spectrum (XPS) was measured by a VG ESCALAB MKIIX-ray photoelectron spectrometer using Mg−Kα as the exciting source (1253.6 eV). Powder X-ray diffraction (XRD) patterns between 10 and 80° (~2θ) were collected by Rigaku D/MAX-2500 powder diffractometer with Cu−Kα radiation (λ = 0.154 nm) operated at 40 kV, 200 mA. Hitachi-SU8030 field emission scanning electron microscope (FESEM, Japan), under the acceleration voltage of 2 kV, was employed and further confirmed on Hitachi-7650 transmission electron microscopy (TEM, Japan) at 80 kV. The chemical composition of the products was characterized by 7539-H energy-dispersive X-ray spectroscopy (EDX, Horiba, England). FTIR transmission spectra from 400 to 4000 cm^{-1} were collected by EQUINOX55 FTIR Spectrometer operated at resolution ratio of 4 cm^{-1} with the KBr technique. The specific surface area (SSA) and pore size distribution were investigated with nitrogen cryosorption (Micromeritics, ASAP2020).

2.3. Electrochemical Measurements. The electrodes were composed of 85 wt % synthesized samples, 10 wt % acetylene carbon black, and 5 wt % PTFE binder (60% suspension in water). A slurry consisting of above mixture was smeared into a 1 × 1 cm area nickel foam (6 M KOH) or platinum mesh (1 M H_2SO_4) with a loading amount of 4 mg cm^{-2}, and dried in vacuum at 120 °C for 12 h. Electrochemical investigations were carried out in three-electrode systems using platinum as counter electrodes and Hg/HgO (0.1 M KOH) as reference electrodes in 6 M KOH; reference electrodes were replaced with Hg/Hg_2Cl_2 (SCE) in 1 M H_2SO_4. The frequency range of 10^5 Hz to 10^{-2} Hz and an ac modulation of 5 mV were used when recording electrochemical impedance spectroscopy (EIS) spectra. Both cyclic voltammetry (CV) and EIS were tested on CHI660A electrochemical workstation (Chenhua, China). Galvanostatical charge−discharge tests were conducted at different densities in 6 M KOH vs Hg/HgO, 1 M H_2SO_4 vs SCE, using computer controlled cycling equipment (Land CT2001A, China). The electrode capacitance was calculated from the following equation:

$$C = \frac{I}{m\frac{dV}{dt}}$$

where I (A) is the discharge current, m (g) is the mass of active materials, and $(dV)/(dt)$ (V s^{-1}) is the gradient of discharge curves.

Galvanostatic charge−discharge cycles of two-electrode cells were measured in 1 M H_2SO_4, using a glassy fibrous separator and foam nickel mesh current collector at a current density of 0.1−3 A g^{-1} between 0−1.1 V. The power density (P) and the energy density (E) of supercapacitors were calculated from the equations $P = E/t$ and $E = {}^1/_2\ CV^2$, respectively, where C is the specific capacitance calculated from the charge−discharge curves, and t is the discharged time.

3. RESULTS AND DISCUSSION

The synthetic approach of 3D HPC is illustrated in Figure 1. The phase composition and crystal structure of as-prepared

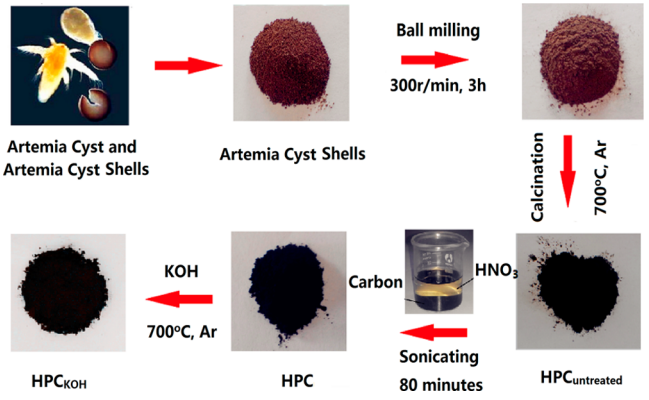

Figure 1. Illustration of a synthetic approach for HPC.

samples were investigated by XRD patterns, as shown in Figure 2a. All XRD patterns show a broad Bragg reflection at around 2θ of 26° which should be attributed to the (002) reflection of a graphitic-type lattice. A weak reflection centered around 43° corresponds to a superposition of the (100) and (101) reflections of a graphitic-type carbon structure, indicating the amorphous nature of the samples. Some small peaks attributed to the impurities were also observed in XRD patterns of $HPC_{untreated}$; however, they disappeared in the patterns of HPC and HPC_{KOH}. This suggests that some acid or alkali dissolvable impurities from the original Artemia cyst shells can be removed after the HNO_3 treatment and KOH activation. Also, such removal can introduce more micro- and mesopores in the macropore walls of carbon frameworks, leading to a hierarchical porous structure. An EDX spectrum (Figure 2b) of $HPC_{untreated}$ indicates the impurity elements are mainly Mg, P, Ca, and Fe.

Nitrogen sorption at 77 K further confirms the hierarchical porous structure of the as- prepared samples. The isotherm plots shown in Figure 2c indicate that the microporous (≤2 nm) structure is predominant in all the samples. The total Brunauer−Emmett−Teller (BET) SSA of HPC is 455 m^2 g^{-1}, of which 73.8% is contributed by the micropore according to the t-plot analysis. Further activation of HPC with KOH can dramatically increase the SSA to 1758 m^2 g^{-1} (Table 1), and an even higher micropore percentage (78.7%) occurs. Meanwhile, the average Barrett−Joyner−Halenda (BJH) pore size drops from 5.78 nm of HPC to 2.62 nm of HPC_{KOH}, which further indicates that KOH activation mainly introduces micropores to the system. Figure 2d shows the BJH pore size distribution of all samples below 10 nm.

DOI: 10.1021/am506815f
ACS Appl. Mater. Interfaces 2015, 7, 1132−1139

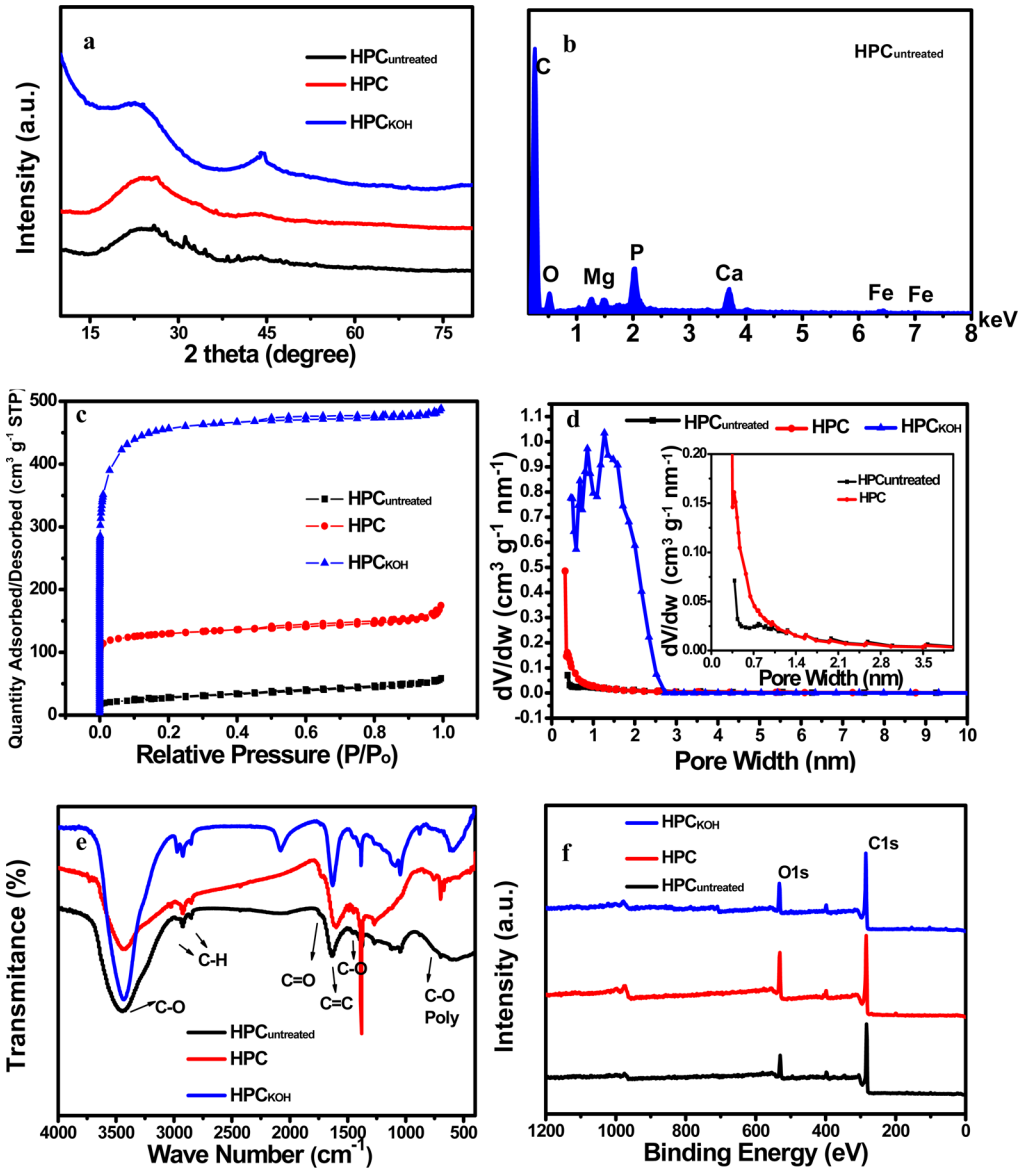

Figure 2. (a) XRD patterns, (b) EDX spectra, (c) isotherm plots, (d) BJH pore size distribution, (e) FTIR spectra, and (f) XPS survey spectra of as-prepared samples.

Table 1. Specific Surface Area, Pore Size, and Pore Volume of All Samples

sample	pore volume ($cm^3\ g^{-1}$)	micropore volume ($cm^3\ g^{-1}$)	BJH pore size (nm)	BET SSA ($m^2\ g^{-1}$)	BET_{micro} SSA ($m^2\ g^{-1}$)
$HPC_{untreated}$	0.09	0.01	4.82	95	18
HPC	0.26	0.16	5.78	455	310
HPC_{KOH}	0.76	0.54	2.62	1758	1384

The FTIR analysis (Figure 2e) was performed to determine the functional groups, especially the oxygen-containing groups, and all of the as-prepared samples show similar peaks. The strong characteristic peak at 3435 cm^{-1} is attributed to the stretching vibration of the O−H bond, and the small peaks at 2917 and 2840 cm^{-1} originated from the stretching vibration of the C−H bond. The peak at 1380 cm^{-1} corresponds to the stretching vibration of C−O bond. The peaks at 1700 and 1623 cm^{-1} are due to the stretching vibration of carboxyl groups C═O and C═C bond.

Further detailed information about surface functionalities was investigated by X-ray photoelectron spectroscopy (XPS) and all the as prepared samples present high oxygen content. Survey spectra of the carbonized products are shown in Figure 2f. The atom ratio of C to O is calculated and listed in Table 2. The HNO_3 treatment can thus introduce more oxygen content to the carbon framework, while oxygen is slightly decreased after KOH activation. The deconvolution of the C 1s and O 1s peaks (Figure S1, Supporting Information) reveal the distribution of oxygen functionalities, which is listed in Table 2. From result of the O 1s deconvolution, it is noticed that most of the oxygen is chemically bonded to carbon framework, only a very few amount of the oxygen is physically absorbed.

More structural details were investigated with SEM observations. The original and ball-milled Artemia cyst shells (Figure 3a−c) show a hierarchical porous structure with different diameter levels from 400 to 800 nm. This structure is well preserved in as-prepared $HPC_{untreated}$ (Figure 3d) and HPC (Figure 3e) but a bit collapsed in HPC_{KOH} (Figure 3f). Further

DOI: 10.1021/am506815f
ACS Appl. Mater. Interfaces 2015, 7, 1132−1139

Table 2. Physical Properties of As-Prepared Samples

	atomic %							
sample	C	O	C−OR,OH[a]	C=O[a]	COOR[a]	C=O[b]	C−OH[b]	O_2/H_2O[b]
$HPC_{untreated}$	76.7	11.5	21.2	4.5	7.5	6.5	91.3	2.3
HPC	77.9	17.3	20.7	4.2	7.8	6.2	91.9	2.0
HPC_{KOH}	78.8	13.1	22.4	3.4	7.7	29.0	66.9	4.1
	binding energy (eV)							
	C−OR,OH[a]	C=O[a]	COOR[a]	C=O[b]	C−OH[b]	O_2/H_2O[b]		
	286.2 ± 0.2	287.6 ± 0.2	288.9 ± 0.2	531 ± 0.2	532 ± 0.2	535 ± 0.2		

[a]Molar ratio of functional groups derived from C 1s XPS peak. [b]Molar ratio of functional groups derived from O 1s XPS peak

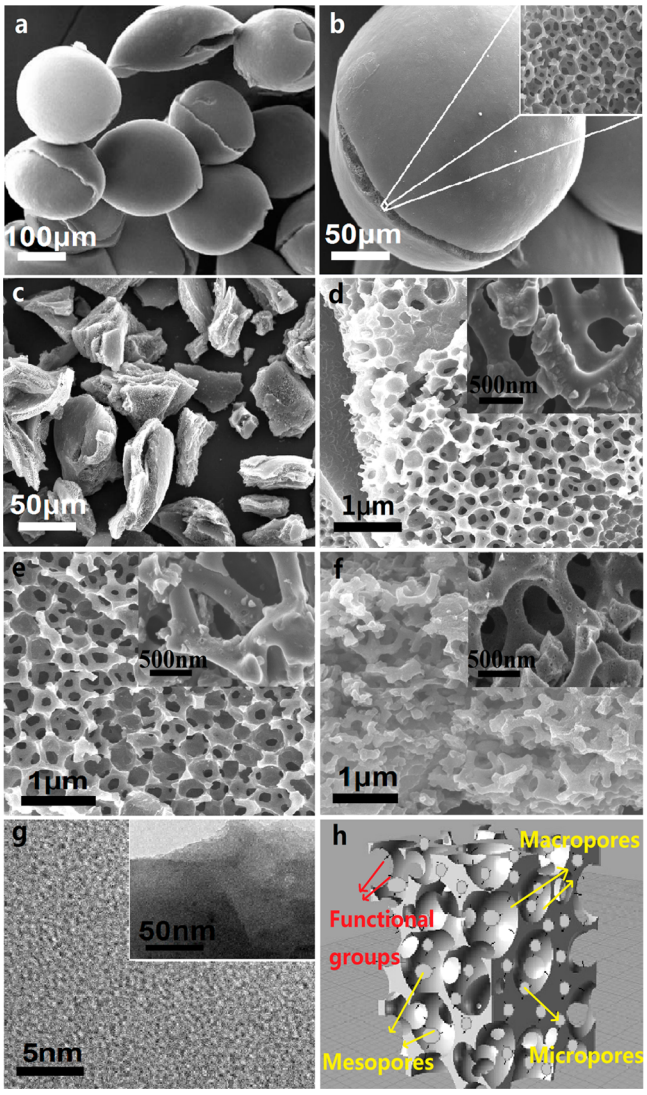

Figure 3. SEM pictures of (a and b) Artemia cyst shells, (c) ball-milled Artemia cyst shells, (d) $HPC_{untreated}$, (e) HPC, (f) HPC_{KOH}, (g) TEM images of HPC, and (h) illustration of 3D HPC.

examine the structure at higher magnification (Figure 3d–f, inset), it can be found that the surface of the carbon frame becomes rough after HNO_3 treatment, and small pores are created on the surface of HPC_{KOH}. A high-resolution TEM picture (Figure 3g) of HPC is also taken to examine the phase composition, and a typical amorphous carbon morphology is observed, which is consistent with XRD results. Figure 3h illustrates the hierarchical porous structure of carbon with abundant functional groups.

To evaluate the energy storage properties of these hierarchical porous carbon materials, we performed a series of electrochemical measurements. The comparative CV plots of all the samples at a scan rate of 10 mV s^{-1} in 6 M KOH are shown in Figure 4a. Apparently, after HNO_3 treatment, the HPC sample presents better capacitance behavior and can be further enhanced in HPC_{KOH}. Bumps representing electrochemical capacitance caused by redox reactions are observed in the CV curves of all the samples, which should be attributed to the oxygenated functional groups on the carbon frameworks. All these CV curves exhibit quasi-rectangular-like mirror image characteristics of capacitive behaviors with respect to the zero-current line, which indicates good capacitive behaviors. Figure 4b demonstrates the galvanostatic charge/discharge curves tested at current density of 0.5 A g^{-1}. Nearly linear and symmetric charge/discharge profiles were obtained for all of the samples, which is consistent with the results of CV measurements. The SC values at different current densities are calculated and shown in Figure 4c. Compared to $HPC_{untreated}$, HPC presents a much higher SC of 297 F g^{-1} at low current density (0.5 A g^{-1}), which remains 263 F g^{-1} at current density of 10 A g^{-1}, indicating the rapid ion transport characteristics probably due to the well interconnected hierarchical porous structure.

Note that the as-prepared carbon materials present relatively low SSA values as compared to commercial activated carbon (typically larger than 2000 m^2g^{-1}), however higher specific capacitance is achieved. This good capacitive behavior should be attributed to combined contribution from pseudocapacitance caused by the oxygen-functional groups and its unique 3D hierarchical porous structure. The abundance of carbonyl (C=O) group on HPC contributed to a high pseudocapacitance due to the following reaction:[43]Meanwhile, the unique

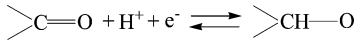

3D hierarchical porous structure of HPC is favorable for the efficient utilization of the active surface area and contributes sufficient double layer capacitance. First, the HPC possesses a large number of micropores with a size of around 0.6–0.8 nm, which are accessible by desolvated aqueous electrolyte ions,[44] do not waste too much extra space. There is an inspiration that, for the design of HPC, the number of these micropores with proper diameters could be further enlarged to contribute greater double layer capacitance. The reasonable amount of mesopores and the interconnected macropores, on the other hand, provide effective ion pathways for ion penetration and transport into the interior of the micropores with a shorter ion diffusion distance as well as a reduced inner resistance. In addition, the abundance of hydrophilic oxygen functional

DOI: 10.1021/am506815f
ACS Appl. Mater. Interfaces 2015, 7, 1132–1139

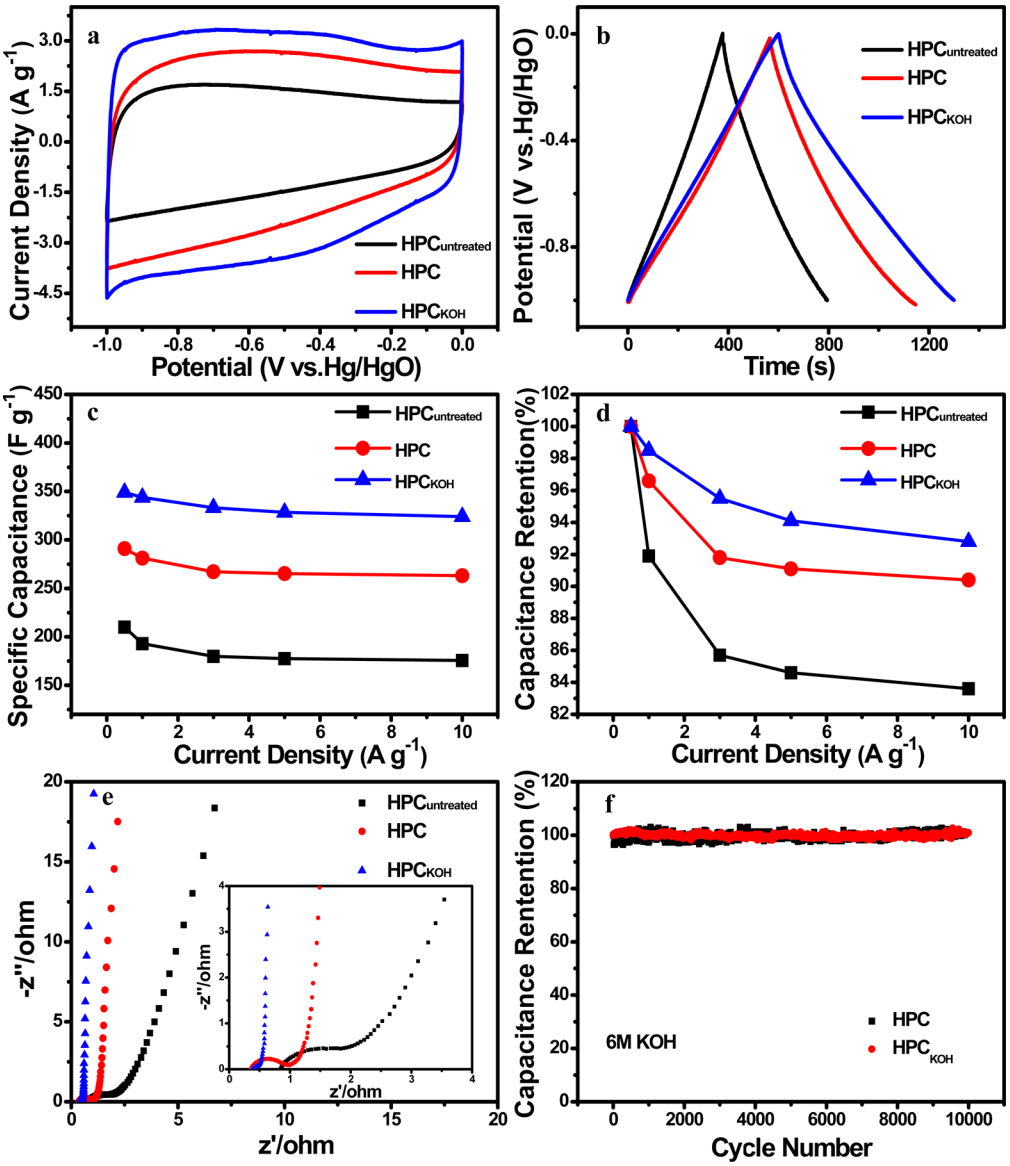

Figure 4. (a) CV curves of as-prepared samples at a scan rate of 10 mV s^{-1} in 6 M KOH; (b) charge/discharge curves of as-prepared samples at a current density of 0.5 A g^{-1} in 6 M KOH; (c) SC values of as-prepared samples at different current densities in 6 M KOH; (d) capacitance retention ratio as a function of discharge current densities; (e) Nyquist plots of as-prepared samples; and (f) cycle stability of HPC and HPC_{KOH} in 6 M KOH.

groups on the carbon frameworks not only contributes pseudocapacitance, but also significantly improves the hydrophilic property of the electrode, which is also beneficial to capacitance behavior in aqueous electrolytes.

It is also noteworthy that after the HNO_3 treatment the SC of HPC is significantly improved from 210 to 297 F g^{-1} (Figure 4c), which is 41.4% higher than that of $HPC_{untreated}$. As mentioned above, large amount of porous structures can be developed with the HNO_3 treatment, leading to a great increase of SSA (Table 1). Although, the HNO_3 treatment mostly contributes to $S_{micro,}$ the good wettability benefited from the rich oxygen content, and the fast ion transport benefited from the interconnected hierarchical porous structure that enable those desolvated ions to enter the HPC micropores more easily. This causes a drastic increase on the numbers of ions absorbed on the carbon surface.[42] These desolvated ions would contribute to the EDLC capacitance.[42] On the other hand, many inorganic/organic impurities can be removed with the HNO_3 treatment, which not only generates considerable porous structures, but also expose the functional groups in the carbon wall to the pore surfaces. Such exposed functional groups can be more effectively utilized and hence contribute more pseudocapacitance, which causes the big bump on the CV curve of HPC (Figure 4a). Therefore, the greatly enhanced performance should result from the combined effect of the increased SSA and exposed functional groups.

Further activation of HPC with KOH leads to a dramatic increase in SC from 297 to 349 F g^{-1} at a current density of 0.5 A g^{-1}, which should be attributed to the dramatic increase of SSA (Table 1). This value retains 324 F g^{-1} at 10 A g^{-1}, suggesting a capacitance retention of 92.8% (Figure 4c). This result reveals that the capacitive performance can be further enhanced through chemical activation. However, the incremental SC value is not proportional to that of SSA, indicating some of the pore sizes resulted from KOH activation are not desirable for supercapacitance. This is probably due to the fact that the KOH activation usually creates micropores, some of which cannot be entered by the electrolyte because the pore

DOI: 10.1021/am506815f
ACS Appl. Mater. Interfaces 2015, 7, 1132−1139

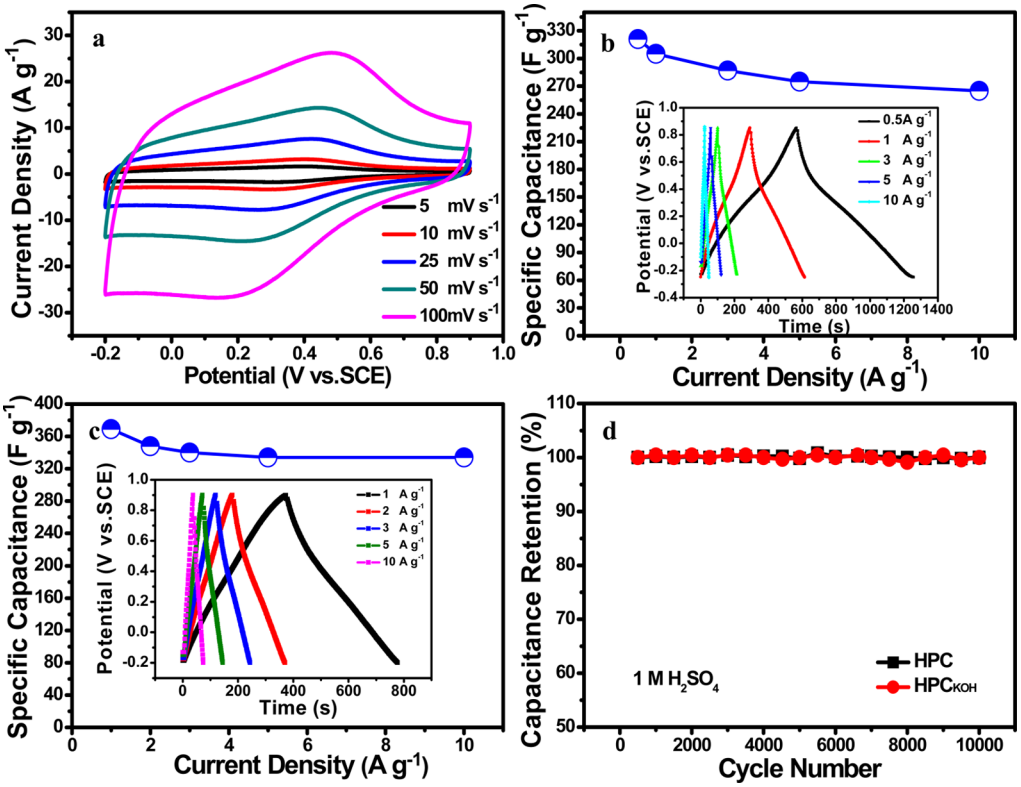

Figure 5. (a) Cyclic voltammetry curves of HPC in 1 M H_2SO_4 at different scan rates; (b) specific capacitance of HPC in 1 M H_2SO_4 at different current densities and (inset) galvanic charge/discharge curves; (c) HPC_{KOH} in 1 M H_2SO_4 at different current densities and (inset) galvanic charge/discharge curves; and (d) cycle performance of HPC and HPC_{KOH} in 1 M H_2SO_4 at current density of 10 A g^{-1}.

Table 3. Comparison of Electrochemical Performance of Carbon from Different Natural Carbon Sources

carbon source	electrolyte	mass (mg)	C_m (F g^{-1})	current density (A g^{-1})	cycling stability (%)
seaweed[39]	H_2SO_4	10−12	255 (three-electrode)	0.2	
seaweed[39]	KOH	10−12	201 (three-electrode)	0.2	
fungi[38]	KOH		196(three-electrode)	0.167	
animal bone[36]	KOH		185 (two-electrode)	0.05	
microalgae[47]	LiCl	11−14	200 (two-electrode)	0.1	98 (10000 cycles)
human hair[48]	KOH	4	340 (three-electrode)	1	98 (20000 cycles)
protein[49]	H_2SO_4	1	390 (three-electrode)	0.25	93 (10000 cycles)
artemia cyst shell	KOH	4	349 (three-electrode)	0.5	100 (10000 cycles)
	H_2SO_4	4	369 (three-electrode)	0.5	100 (10000 cycles

size is too small or not in an appropriate shape, which can be confirmed by the much smaller average BJH pore size of HPC_{KOH} (Table 1).

Figure 4e shows the Nyquist plots of $HPC_{untreated}$, HPC and HPC_{KOH} tested under the ac modulation of 5 mV over the frequency range of 10^{-2}−10^5 Hz. The ohmic resistance of HPC and HPC_{KOH} is obviously lower than that of $HPC_{untreated}$. Both HPC and HPC_{KOH} show a near-vertical curve in the low frequency region, indicating a good capacitor behavior, especially for HPC_{KOH}. In the high-frequency region, a larger semicircle represents larger charge transfer resistance (CTR) and a larger *x*-intercept represents larger equivalent series resistance (ESR). Both HPC and HPC_{KOH} have lower CTR and ESR than that of $HPC_{untreated}$, which should be attributed to the interconnected 3D porous structure that facilitate contact between the ion and the material.[29]

On the basis of conventional knowledge, the oxygen-functional groups can greatly increase the SC value by introducing pseudocapacitance, but they are also often detrimental to cyclability.[30] Therefore, long-term stability of this material is not certain. The long cycle performance of HPC was tested using a three-electrode system (Figure 4f). Unexpectedly, HPC shows an excellent cycling stability, and 100% capacitance retention is achieved upon 10000 charge/discharge cycles for all the samples. In fact, Yang et al.[45] observed that the heteroatoms on the carbon framework brought from the original precursor, rather than post treated with chemical or physical methods, can usually stay stable under harsh working conditions. This is consistent with our results. To examine the electrochemical performance of the HPCs in strong acidic electrolyte, the capacitance behavior of HPC and HPC_{KOH} was also tested using 1 M H_2SO_4 as electrolyte, as shown in Figure 5. An even higher SC of 369 F g^{-1} is achieved for HPC_{KOH} at current density of 0.5 A g^{-1} in 1 M H_2SO_4, and still remains 334 F g^{-1} at 10 A g^{-1} with a good capacitance retention of 91%. Note that the SC values in KOH for both HPC and HPC_{KOH} are much smaller than that in H_2SO_4. This phenomenon can be explained according to the

DOI: 10.1021/am506815f
ACS Appl. Mater. Interfaces 2015, 7, 1132−1139

theory of Andreas and Conway,[46] where the pseudofaradic contribution of oxygenated surface functionalities is less efficient in alkaline than in acid medium, and nearly negligible at neutral pH. This is also consistent with the CV results. Besides, both HPC and HPC_{KOH} exhibit an excellent long life cycle (100% after 10 000 charge/discharge cycles), indicating that the electrode has a good electrochemical stability and a high degree of reversibility in both acidic and alkaline electrolytes. Figure S3b (Supporting Information) shows the Coulombic efficiency as a function of cycle number in H_2SO_4, which varies from 1.02 to 0.99, and after 10 000 cycles, Coulombic efficiency of HPC and HPC_{KOH} was still close to 1, further indicating good cycle stability. It is noticeable that, the SC values of both HPC and HPC_{KOH} are distinguished as compared to those carbon derived from varies of carbon resources (Table 3). The performance of symmetric supercapacitors based on HPC_{KOH} in 1 M H_2SO_4 was also tested (Figure S4, Supporting Information). A relatively high energy density of 12.9 Wh kg^{-1} is obtained at power density of 55 W kg^{-1} in 1 M H_2SO_4 electrolyte, which remains 11.4 Wh kg^{-1} at power density of 1658 W kg^{-1}.

4. CONCLUSIONS

High-performance supercapacitor electrode materials were developed through a green and low-cost carbonization method. The combined 3D hierarchical porous structure and oxygen rich properties enable these materials exhibit high SC, excellent cycle stability, and promising rate performance. This suggests the possibility of the designing of high-performance carbon electrodes with certain pore size distribution in aqueous electrolyte. Finding or synthesizing carbon precursors with functional groups can provide high and stable pseudocapacitance. Also, for the design of hierarchical porous carbon for aqueous supercapacitors, micropores with proper pore size could be predominant to ensure the full utilization of effective surface area. Moreover, the interconnection of macropores is beneficial to the adsorption of electrolytes into the micropores.

■ ASSOCIATED CONTENT

Supporting Information

Fitting results on C 1s and O 1s from XPS spectra of as-prepared samples; CV curves of HPC and HPC_{KOH} at different scan rates in 6 M KOH; galvanic charge/discharge curves of HPC and HPC_{KOH} at different current densities in 6 M KOH; CV curves of HPC activated at different (W_{HPC}:W_{KOH}) ratio at a scan rate of 10 mV s^{-1} in 6 M KOH; the Coulombic efficiency of HPC and HPC_{KOH} as a function of cycle number in H_2SO_4; and electrochemical performance of the symmetric capacitor of HPC_{KOH} in 1 M H_2SO_4. This material is available free of charge via the Internet at http://pubs.acs.org.

■ AUTHOR INFORMATION

Corresponding Authors

*E-mail: yufengzhao@ysu.edu.cn.
*E-mail: jinsong-wu@northwestern.edu.

Notes

The authors declare no competing financial interest.

■ ACKNOWLEDGMENTS

Financial support from the NSFC (Grant 51202213), NSFHBP (Grant B2012203043), CPSF (Grant 2013M530889, 2014T70230) and EYSFHP (Grant Y2012005) is acknowledged.

■ REFERENCES

(1) Zhai, Y.; Dou, Y.; Zhao, D.; Fulvio, P. F.; Mayes, R. T.; Dai, S. Carbon Materials for Chemical Capacitive Energy Storage. *Adv. Mater.* **2011**, *23*, 4828−4850.
(2) Verbrugge, M. W.; Liu, P.; Soukiazian, S. Activated-Carbon Electric-Double-Layer Capacitors: Electrochemical Characterization and Adaptive Algorithm Implementation. *J. Power Sources* **2005**, *141*, 369−385.
(3) Ma, R. Z.; Liang, J.; Wei, B. Q.; Zhang, B.; Xu, C. L.; Wu, D. H. Study of Electrochemical Capacitors Utilizing Carbon Nanotube Electrodes. *J. Power Sources* **1999**, *84*, 126−129.
(4) Li, W. C.; Reichenauer, G.; Fricke, J. Carbon Aerogels Derived from Cresol-Resorcinol Formaldehyde for Supercapacitors. *Carbon* **2002**, *40*, 2955−2959.
(5) Gogotsi, Y.; Nikitin, A.; Ye, H.; Zhou, W.; Fischer, J. E.; Yi, B.; Foley, H. C.; Barsoum, M. W. Nanoporous Carbide-Derived Carbon with Tunable Pore Size. *Nat. Mater.* **2003**, *2*, 591−594.
(6) Chmiola, J.; Yushin, G.; Gogotsi, Y.; Portet, C.; Simon, P.; Taberna, P. L. Anomalous Increase in Carbon Capacitance at Pore Sizes Less Than 1 Nanometer. *Science* **2006**, *313* (5794), 1760−1963.
(7) Frackowiak, E.; Béguin, F. Carbon Materials for The Electrochemical Storage of Energy in Capacitors. *Carbon* **2001**, *39*, 937−950.
(8) Pandolfo, A. G.; Hollenkamp, A. F. Carbon Properties and Their Role in Supercapacitors. *J. Power Sources* **2006**, *157*, 11−27.
(9) Xing, W.; Huang, C. C.; Zhuo, S. P.; Yuan, X.; Wang, G. Q.; Hulicova-Jurcakova, D.; Yan, Z. F.; Lu, G. Q. Hierarchical Porous Carbons with High Performance for Supercapacitor Electrodes. *Carbon* **2009**, *47*, 1715−1722.
(10) Feng, X. L.; Liang, Y. Y.; Zhi, L. J.; Thomas, A.; Wu, D. Q.; Lieberwirth, I.; Kolb, U.; Müllen, K. Synthesis of Microporous Carbon Nanofibers and Nanotubes from Conjugated Polymer Network and Evaluation in Electrochemical Capacitor. *Adv. Funct. Mater.* **2009**, *19*, 2125−2129.
(11) Inagaki, M.; Yang, Y.; Kang, F. Carbon Nanofibers Prepared via Electrospinning. *Adv. Mater.* **2012**, *24*, 2547−2566.
(12) Zhao, Y. F.; Wang, W.; Xiong, D. B.; Shao, G. J.; Xia, W.; Yu, S. X.; Gao, F. M. Titanium Carbide Derived Nanoporous Carbon For Supercapacitor Applications. *Int. J. Hydrogen Energy* **2012**, *37*, 19395−19400.
(13) Stoller, M. D.; Park, S. J.; Zhu, Y. W.; An, J. H.; Ruoff, R. S. Graphene-Based Ultracapacitors. *Nano Lett.* **2008**, *8*, 3498−3502.
(14) Liu, H. J.; Wang, J.; Wang, C. X.; Xia, Y. Y. Ordered Hierarchical Mesoporous/Microporous Carbon Derived from Mesoporous Titanium-Carbide/Carbon Composites and its Electrochemical Performance in Supercapacitor. *Adv. Energy Mater.* **2011**, *1*, 1101−1108.
(15) Korenblit, Y.; Rose, M.; Kockrick, E.; Borchardt, L.; Kvit, A.; Kaskel, S.; Yushin, G. High-Rate Electrochemical Capacitors Based on Ordered Mesoporous Silicon Carbide-Derived Carbon. *ACS Nano* **2010**, *4*, 1337−1344.
(16) Carriazo, D.; Picó, F.; Gutiérrez, M. C.; Rubio, F.; Rojo, J. M.; Monte, F. D. Block-Copolymer Assisted Synthesis of Hierarchical Carbon Monoliths Suitable As Supercapacitor Electrodes. *J. Mater. Chem.* **2010**, *20*, 773−780.
(17) Liang, Y.; Feng, X.; Zhi, L.; Kolb, U.; Müllen, K. A Simple Approach towards One-Dimensional Mesoporous Carbon with Superior Electrochemical Capacitive Activity. *Chem. Commun.* **2009**, 809−811.
(18) Wang, D. W.; Li, F.; Liu, M.; Lu, G. Q.; Cheng, H. M. Synthesis and Dye Separation Performance of Ferromagnetic Hierarchical Porous Carbon. *Carbon* **2008**, *46*, 1593−1599.
(19) Chen, Z. P.; Ren, W. C.; Gao, L. B.; Lu, B. L.; Pei, S. F.; Cheng, H. M. Three-Dimensional Flexible and Conductive Interconnected Graphene Networks Grown by Chemical Vapour Deposition. *Nat. Mater.* **2011**, *10*, 424−428.

DOI: 10.1021/am506815f
ACS Appl. Mater. Interfaces 2015, 7, 1132−1139

(20) Rakhi, R. B.; Chen, W.; Cha, D.; Alshareef, H. N. Nanostructured Ternary Electrodes for Energy-Storage Applications. *Adv. Energy Mater.* **2012**, *2*, 381−389.
(21) You, B.; Jiang, J. H.; Fan, S. J. Three-Dimensional Hierarchically Porous All-Carbon Foams for Supercapacitor. *ACS Appl. Mater. Interfaces* **2014**, *6*, 15302−15308.
(22) Hulicova-Jurcakova, D.; Puziy, A. M.; Poddubnaya, O. I.; Suárez-García, F.; Tascón, J. M. D.; Lu, G. Q. Highly Stable Performance of Supercapacitors from Phosphorus-Enriched Carbons. *J. Am. Chem. Soc.* **2009**, *131*, 5026−5027.
(23) Hulicova-Jurcakova, D.; Seredych, M.; Lu, G. Q.; Bandosz, T. J. Combined Effect of Nitrogen- and Oxygen-Containing Functional Groups of Microporous Activated Carbon on its Electrochemical Performance in Supercapacitors. *Ad. Funct. Mater.* **2009**, *19*, 438−447.
(24) Béguin, F.; Szostak, K. A Self-Supporting Electrode for Supercapacitors Prepared by One-Step Pyrolysis of Carbon Nanotube/Polyacrylonitrile Blends. *Adv. Mater.* **2005**, *17*, 2380−2384.
(25) Stein, A.; Wang, Z. Y.; Fierke, M. A. Functionalization of Porous Carbon Materials with Designed Pore Architecture. *Adv. Mater.* **2009**, *21*, 265−293.
(26) Chen, L. F.; Zhang, X. D.; Liang, H. W.; Kong, M.; Guan, Q. F.; Chen, P.; Wu, Z. Y.; Yu, S. H. Synthesis of Nitrogen-Doped Porous Carbon Nanofibers as an Efficient Electrode Material for Supercapacitors. *ACS Nano* **2012**, *6*, 7092−7102.
(27) Li, H.; Cheng, N.; Zheng, Y.; Zhang, X.; Lv, H.; He, D.; Pan, M.; Kleitz, F.; Qiao, S.; Mu, S. C. Oxidation Stability of Nanographite Materials. *Adv. Energy Mater.* **2013**, *3*, 1176−1179.
(28) Li, Z.; Xu, Z.; Tan, X.; Wang, H.; Holt, C. M. B.; Stephenson, T.; Olsen, B. C.; Mitlin, D. Mesoporous Nitrogen-Rich Carbons Derived from Protein for Ultra-High Capacity Battery Anodes and Supercapacitors. *Energy Environ. Sci.* **2013**, *6*, 871−878.
(29) Qie, L.; Chen, W.; Xu, H.; Xiong, X.; Jiang, Y.; Zou, F.; Hu, X. L.; Xin, Y.; Zhang, Z. L.; Huang, Y. H. Synthesis of Functionalized 3D Hierarchical Porous Carbon for High-Performance Supercapacitors. *Energy Environ. Sci.* **2013**, *6*, 2497−2504.
(30) Simon, P.; Gogotsi, Y. Materials for Electrochemical Capacitors. *Nat. Mater.* **2008**, *7*, 845−854.
(31) Guo, Y. P.; Qi, J. R.; Jiang, Y. Q.; Yang, S. F.; Wang, Z. C.; Xu, H. D. Performance of Electrical Double Layer Capacitors with Porous Carbons Derived From Rice Husk. *Mater. Chem. Phys.* **2003**, *80* (3), 704−709.
(32) Kuratani, K.; Okuno, K.; Iwaki, T.; Kato, M.; Takeichi, N.; Miyuki, T.; Awazu, T.; Majima, M.; Sakai, T. Converting Rice Husk Activated Carbon into Active Material for Capacitor Using Three-dimensional Porous Current Collector. *J. Power Sources* **2011**, *196*, 10788−10790.
(33) Peng, C.; Yan, X.; Wang, R.; Lang, J.; Ou, Y.; Xue, Q. Promising Activated Carbons Derived from Waste Tea Leaves and Their Application in High Performance Supercapacitors Electrodes. *Electrochim. Acta* **2013**, *87*, 401−408.
(34) Goodman, P. A.; Li, H.; Gao, Y.; Lu, Y. F.; Stenger-Smith, J. D.; Redepenning, J. Preparation and Characterization of High Surface Area, High Porosity Carbon Monoliths from Pyrolyzed Bovine Bone and Their Performance as Supercapacitor Electrodes. *Carbon* **2013**, *55*, 291−298.
(35) Ismanto, A. E.; Wang, S.; Soetaredjo, F. E.; Ismadji, S. Preparation of Capacitor's Electrode from Cassava Peel Waste. *Bioresour. Technol.* **2010**, *101*, 3534−3540.
(36) Huang, W. T.; Zhang, H.; Huang, Y. Q.; Wang, W. K.; Wei, S. C. Hierarchical Porous Carbon Obtained from Animal Bone and Evaluation in Electric Double-Layer Capacitors. *Carbon* **2011**, *49*, 838−843.
(37) Lv, Y. K.; Gan, L. H.; Liu, M. X.; Xiong, W.; Xu, Z. J.; Zhu, D. Z.; Wright, D. S. A Self-Template Synthesis of Hierarchical Porous Carbon Foams Based on Banana Peel for Supercapacitor Electrodes. *J. Power Sources* **2012**, *209*, 152−157.
(38) Zhu, H.; Wang, X. L.; Yang, F.; Yang, X. R. Promising Carbons for Supercapacitors Derived from Fungi. *Adv. Mater.* **2011**, *23*, 2745−2748.
(39) Bichat, M. P.; Raymundo-Piñero; Béguin, E. F. High Voltage Supercapacitor Built with Seaweed Carbons in Neutral Aqueous Electrolyte. *Carbon* **2010**, *48* (15), 4351−4361.
(40) Wang, S. F.; Sun, S. C. Comparative Observations on the Cyst Shells of Seven Artemia Strains from China. *Microsc. Res. Tech.* **2007**, *70*, 663−670.
(41) Sorgeloos, P.; Bossuyt, E.; Laviña, E.; Baeza-Mesa, M.; Persoone, G. Decapsulation of Artemia Cysts: A Simple Technique for the Improvement of the Use of Brine Shrimp in Aquaculture. *Aquaculture* **1977**, *12*, 311−315.
(42) Hsieh, C. T.; Teng, H. Influence of Oxygen Treatment on Electric Double-Layer Capacitance of Activated Carbon Fabrics. *Carbon* **2002**, *40*, 667−674.
(43) Chen, C. M.; Zhang, Q.; Zhao, X. C.; Zhang, B. S.; Blume, R.; Kong, Q. Q.; Yang, M. G.; Yang, Q. H.; Wang, M. Z.; Yang, Y. G.; Schlögl, R.; Su, D. S. Hierarchical Aminated Graphene Based Honeycombs as Supercapacitor Electrode. *J. Mater. Chem.* **2012**, *22*, 14076−14084.
(44) Chmiola, J.; Yushin, G.; Dash, R. K.; Hoffman, E. N.; Fischer, J. E.; Barsoum, M. W.; Gogotsi, Y. Double-Layer Capacitance of Selected Carbide Derived Carbons in Sulfuric Acid. *Electrochem. Solid-State Lett.* **2005**, *8*, A357−A360.
(45) Yang, X.; Wu, D.; Chen, X.; Fu, R. Nitrogen-Enriched Nanocarbons with a 3-D Continuous Mesopore Structure from Polyacrylonitrile for Supercapacitor Application. *J. Phys. Chem. C* **2010**, *114*, 8581−8586.
(46) Andreas, H. A.; Conway, B. E. Examination of the Double-Layer Capacitance of an High Specific-Area C-Cloth Electrode as Titrated from Acidic to Alkaline pHs. *Electrochim. Acta* **2006**, *51*, 6510−6520.
(47) Sevilla, M.; Gu, W.; Falco, C.; Titirici, M. M.; Fuertes, A. B.; Yushin, G. Hydrothermal Synthesis of Microalgae-Derived Microporous Carbons for Electrochemical Capacitors. *J. Power Sources* **2014**, *267*, 26−32.
(48) Qian, W.; Sun, F.; Xu, Y.; Qiu, Li.; Liu, C.; Wang, S.; Yan, F. Human Hair-Derived Carbon Flakes for Electrochemical Supercapacitors. *Energy Environ. Sci.* **2014**, *7*, 379−386.
(49) Li, Z.; Xu, H.; Tan, X.; Wang, H.; Holt, C. M. B.; Stephenson, T.; Olsen, B. C.; Mitlin, D. Mesoporous Nitrogen-Rich Carbons Derived from Protein for Ultra-High Capacity Battery Anodes and Supercapacitors. *Energy Environ. Sci.* **2013**, *6*, 871−878.

DOI: 10.1021/am506815f
ACS Appl. Mater. Interfaces 2015, 7, 1132−1139